Howard Ramirez-Malule, Stefan Junne, Mariano Nicolás Cruz Bournazou, Peter Neubauer, Rigoberto Ríos-Estepa

A combined experimental and numerical approach identifies a strong association between TCA cycle intermediate accumulation and clavulanic acid biosynthesis in Streptomyces clavuligerus

A combined experimental and numerical approach identifies a strong association between TCA cycle intermediate accumulation and clavulanic acid biosynthesis in *Streptomyces clavuligerus*

Howard Ramirez-Malule[1], Stefan Junne[2], M. Nicolás Cruz-Bournazou[2], Peter Neubauer[2], Rigoberto Ríos-Estepa[3*]

[1]Escuela de Ingeniería Química, Universidad del Valle, A.A. 25360 Cali, Colombia.

[2]Chair of Bioprocess Engineering, Department of Biotechnology, Technische Universität Berlin, Ackerstr. 76, ACK 24, D-13355 Berlin, Germany.

[3]Grupo de Bioprocesos, Departamento de Ingeniería Química, Universidad de Antioquia UdeA, Calle 70 No. 52-21, Medellín, Colombia.

---

* Corresponding Author:

Email Address: rigoberto.rios@udea.edu.co

Telephone: +57 4 2198568

A combined experimental and numerical approach identifies a strong association between TCA cycle intermediate accumulation and clavulanic acid biosynthesis in *Streptomyces clavuligerus*

Abstract

Clavulanic acid (CA) is produced by *Streptomyces clavuligerus* (*S. clavuligerus*) as a secondary metabolite. It is of pharmaceutical interest due to its potential to inhibit β-lactamases, secreted by bacteria as a defense mechanism against β-lactam antibiotics. Knowledge about the carbon flux distribution along the various routes that supply CA precursors would certainly provide insights concerning how to optimize productivity. In order to evaluate metabolic patterns and the possible accumulation of TCA cycle intermediates during CA biosynthesis, batch and subsequent continuous cultures with steadily declining feed rates were performed with glycerol as the main substrate. The data were used as constraints for an *in silico* study aim at exploring the cell metabolic capabilities and the accumulation of metabolic intermediates. While clavulanic acid accumulated at glycerol excess, it steadily decreased at declining dilution rates; CA synthesis stopped when glycerol became the limiting substrate.

A strong association of succinate, oxaloacetate, malate and acetate accumulation with CA production in *S. clavuligerus* was observed. Furthermore, flux balance analysis (FBA) was used to describe the carbon flux distribution with a 10 % deviation on average. Results coincided with the observed intermediate metabolite consumption and/or accumulation, and clavam metabolism.

Key words: Clavulanic acid; *Streptomyces clavuligerus*; continuous cultivation; TCA cycle intermediate accumulation; flux balance analysis.

Introduction

Clavulanic acid (CA), produced by *Streptomyces clavuligerus* (*S. clavuligerus*), is a secondary metabolite with pharmaceutical interest due to its potential to inhibit β-lactamase enzymes. It is secreted by bacteria as a defense mechanism against β-lactam antibiotics (Brown et al. 1976;

Llarrull et al. 2010). Though CA is produced in submerged cultures under different modes of operation, a higher productivity is achieved in continuous cultivations (Neto et al. 2005). However, only a few studies have been conducted to evaluate cell metabolic performance under different dilution rates (Bushell et al. 2006), although such studies may contribute to a better understanding of CA production in submerged cultures.

In most cases, production of antibiotics is performed at growth-limiting concentrations of inorganic phosphate (Ozcengiz and Demain 2013; Hwang et al. 2014). Phosphate deficiency plays a remarkable role on the availability of the glycolytic precursor glyceraldehyde-3-phosphate (GAP), and indirectly on CA synthesis, since it strongly depends on GAP (Ives and Bushell 1997; Kirk et al. 2000; Bushell et al. 2006).

There are two main steps involved in CA biosynthesis. The early step includes the condensation of GAP and arginine to produce *L*-N^2-(2-carboxy-ethyl) arginine by the action of the enzyme N^2-(2-carboxy-ethyl) arginine synthase (CEAS1/CEAS2) (see Fig. 1) (Khaleeli et al. 1999; Ozcengiz and Demain 2013). Next, the (3S, 5S)-clavaminic acid intermediate is synthesized in five - well known - reactions (Wu et al. 1995; Bachmann et al. 1998; Zhang et al. 2002), while the following ones are not fully described yet (Ozcengiz and Demain 2013).

In Streptomycetes, antibiotic biosynthesis and regulation depends on the availability of precursors, which are intermediates of the TCA cycle (Dekleva and Strohl 1988; Hodgson 2000). Attempting to decipher such a puzzle would require not only data for CA and intermediate carbon flux distribution and accumulation, but also a holistic view of its metabolic connectivity. Such studies can be supported by flux balance analysis (FBA), which has been successfully used to estimate the metabolic flux distribution of entire metabolic networks in diverse organisms (Stephanopoulos et al. 1998; Villadsen et al. 2011; Antoniewicz 2015).

In this work, a combined approach that involves continuous cultivation with *Streptomyces clavuligerus* DSM No 41826 and FBA analysis was used for explaining the TCA cycle flux distribution, accumulation of TCA cycle intermediates and their potential association with CA biosynthesis. The experimental set-up included *S. clavuligerus* cultivations with a chemical defined medium in a batch and subsequent continuous cultivation with steadily declining feeding rates.

Materials and methods

Microorganism

Streptomyces clavuligerus DSM No 41826 was used throughout this work. Stock cultures were stored at -80°C in a glycerol solution (16.7% v/v).

Culture media and experimental conditions

In this work, the seed and bioreactor batch medium, described by Roubos *et al*. (2002) was used. The seed medium composition was (in g/L): glycerol 15, soy peptone 15, sodium chloride 3, and calcium carbonate 1, at an initial pH of 6.8. Antifoam 204 (Sigma Inc., St. Louis, MO) was applied at a concentration of 1:1000 v/v.

The final bioreactor batch medium was slightly modified as follows (in g/L): glycerol 9.3, K_2HPO_4 0.8, $(NH_4)_2SO_4$ 1.26, monosodium glutamate 9.8, $FeSO_4 \times 7H_2O$ 0.18, $MgSO_4 \times 7H_2O$ 0.72, MOPS 10.5 and trace element solution 1.44 (mL). The composition of the trace element solution was (in g/L): H_2SO_4 (96%) 20.4, citrate $\times 1H_2O$ 50, $ZnSO_4 \times 7H_2O$ 16.75, $CuSO_4 \times 5H_2O$ 2.5, $MnCl_2 \times 4H_2O$ 1.5, H_3BO_3 2 and $Na_2MoO_4 \times 2H_2O$ 2. Antifoam 204 was applied at a concentration of 1:1000 v/v. The feed medium had the same composition as the bioreactor batch medium, except for K_2HPO_4 that was added at a concentration of 0.58 g/L, without MOPS. The batch medium was designed for achieving phosphate limitation based on the phosphate/carbon ratio of biomass composition, as reported in previous works (Roubos 2002; Roubos et al. 2002)

Cryotube cell suspensions (1.2 mL) were inoculated into 50 mL of seed medium in a 250 mL UltraYield© shake flask (Thomson Instrument Company, Oceanside, CA). Cells were grown in a rotary shaker incubator for 26 h at 200 rpm and 28 °C. For the second preculture, 250 mL UltraYield© shake flasks were filled with 45 mL of bioreactor batch medium and inoculated with 5 mL of cultivated seed broth. Cells were grown for 20 h. The preculture was inoculated at 10% v/v into the bioreactor batch medium.

Culture samples (2 mL) were withdrawn at an interval of approximately 12 h. Samples were centrifuged at 15,000 rpm and 4 °C for 10 min. Supernatant samples were used for CA, intermediate metabolites and glycerol quantification by HPLC-DAD and HPLC-RID (Foulstone and Reading 1982; Junne et al. 2011; Ramirez-Malule et al. 2016a). Wet biomass was washed with 0.9% NaCl and centrifuged. Lastly, test tubes were dried over night at 75 °C for dry cell weight determination.

Continuous cultivation was conducted in a 0.5 L glass-made bioreactor (Glasgerätebau Ochs, Bovenden, Germany) with a working volume of 0.3 L. The reactor was equipped with pH and DO sensors (Hamilton Inc, Bonaduz, Switzerland), a cooling bath for temperature control and an exhaust gas device with an oxygen and carbon dioxide gas sensor BlueInOne Ferm (BlueSens gas sensor GmbH, Herten, Germany). The strain was grown at 28 °C with magnetic stirring, 2 vvm of aeration rate and a constant pH of 6.8, automatically controlled by the addition of HCl (1 M). Air supply was started only 5 h after inoculation in order to initially maintain CO_2 as a co-substrate, and to induce the anaplerotic reaction (carboxylation of phosphoenolpyruvate to oxaloacetate).

After 36 h of cultivation, the batch mode was followed by the continuous feeding phase. The dilution rate (D) was set to 0.050 h^{-1} based on pre-experimental work. After 155 h of cultivation a decrease in the dilution rate was performed with a constant deceleration rate $(\boldsymbol{a})$ of 0.00039 h^{-2} so as to allow the microorganism to adapt to new environmental conditions (quasi-stationary), and eventually obtain information about metabolic patterns at different feeding conditions in a single experiment (Paalme et al. 1995). The dilution rate profile was controlled by the following equation (Paalme et al. 1995):

$$D = D_0 + a * t \qquad (1)$$

in which D is the current dilution rate, D_0 is the initial dilution rate, a is the deceleration rate and t is time.

The specific growth rate μ, product formation I_P, and substrate consumption I_S in continuous culture were determined based on the biomass, product and substrate balance equations, respectively (see equations 2, 3 and 4) (Paalme et al. 1995):

$$\mu = \frac{1}{X_m}\frac{\Delta X}{\Delta \mathrm{t}} + \frac{1}{V_m}\frac{\Delta V}{\Delta \mathrm{t}} + D_m \qquad (2)$$

$$I_p = V_m\frac{\Delta \mathrm{P}}{\Delta \mathrm{t}} + P_m\frac{\Delta V}{\Delta \mathrm{t}} + D_m P_m V_m \qquad (3)$$

$$I_s = V_m\frac{\Delta \mathrm{S}}{\Delta \mathrm{t}} + S_m\frac{\Delta V}{\Delta \mathrm{t}} + D_m V_m (S_0 - S_m) \qquad (4)$$

in which X_m, V_m, D_m, P_m and S_m are the mean values of biomass concentration, volume, dilution rate, product and substrate, between two consecutive data points, respectively; ΔX, $\Delta \mathrm{t}$, ΔV, $\Delta \mathrm{P}$ and $\Delta \mathrm{S}$ are the differences of biomass concentration, time, volume, product and substrate, between two consecutive data points, respectively.

For the batch stage, μ and I_P were quantified by applying equations 5 and 6, respectively (Lee et al. 2009):

$$\mu = \frac{1}{X_m}\frac{\Delta X}{\Delta \mathrm{t}} \quad (5)$$

$$I_p = \frac{1}{X_m}\frac{\Delta \mathrm{P}}{\Delta \mathrm{t}} \quad (6)$$

Analytical Methods

CA was determined by HPLC, using a method based on the work of Foulstone and Reading (1982) and Ramirez-Malule *et al*. (2016a). Potassium clavulanate vetranal (Sigma-Aldrich) was used for calibration. Samples were derivatized with imidazole and analyzed with an Agilent 1200 system (Agilent Technologies, Waldbronn, Germany) equipped with a diode array detector and operated at 30 °C with a Zorbax Eclipse XDB-C-18 reverse phase column ($5\,\mu m, 4.6 \times 150\,mm - Agilent\ Inc, Santa\ Clara, CA$), using a C-18 guard column (Phenomenex®), with a flow rate of 1 mL/min. The mobile phase consisted of solvent A (KH_2PO_4 50 mM, pH 3.2) and solvent B (HPLC grade methanol) was set in a gradient mode as follows: linear gradient from 6% to 10% solvent B for 20 min; linear gradient to 76% solvent B for 22 min; 76% solvent B for 10 min and linear gradient to 6% solvent B for 1 min. The clavulanate-imidazole complex was detected at 311 nm.

Glycerol was quantified with an Agilent 1200 series HPLC system equipped with a refractive index detector and operated at 15 °C with a HyperREZ™ XP carbohydrate H^+ column (thermo scientific) $(300 \times 7.7\,mm, 8\,\mu m)$ at a constant flow rate of 0.5 ml/min using 5 mM sulfuric acid solution as mobile phase. This method was also used to quantify metabolite concentrations from central carbon metabolism, e.g., oxaloacetate, malate, succinate, acetate, lactate, pyruvate, α-ketoglutarate and formate (Junne et al. 2011).

Quantification of free amino acids was performed with an Agilent 1260 series Infinity HPLC system (Agilent Technologies, Waldbronn, Germany), equipped with an Agilent 1200 system fluorescence detector (excitation wavelength: 340 nm, emission wavelength: 450 nm), and operated at 40 °C with a C18 Gemini® column $\left(5\mu, 100\ \text{Å}, 150 \times 4.6mm\right)$, a SecurityGuard™ pre-column (both columns supplied by Phenomenex®, Aschaffenburg, Germany) at a flow rate of 1 mL/min. Ortho-phthaldialdehyde was used for precolumn derivatization as previously reported (Lemoine et al. 2015; Lemoine et al. 2016).

Both, phosphate and ammonium ions, were determined semi-quantitatively using a phosphate and ammonia test (MQuant™, EMD KGaA, Darmstadt, Germany).

Genome Scale Metabolic Modeling of *S. clavuligerus*

The metabolic model reported by Medema *et al*. (2010) was manually curated and used for FBA simulations. The model consisted of the major metabolic pathways i.e., glycolysis, gluconeogenesis, pentose phosphate pathway (PP), tricarboxylic acid cycle (TCA cycle), urea cycle, glyoxylate shunt, anaplerotic reactions, clavam pathway, cephalosporin C biosynthesis, cephamycin C biosynthesis, and the biosynthesis of macromolecular components of biomass (protein, phospholipid, carbohydrate, fatty acid, RNA and DNA). The published model has 1492 reactions (1290/202 internal/exchange fluxes) and 1173 metabolites (971/202 internal/external metabolites) (Medema et al. 2010).

For curation purposes, the model was tested and modified according to open scientific literature (Roubos 2002; Arulanantham et al. 2006; Bushell et al. 2006; Ozcengiz and Demain 2013), public databases like the KEGG pathway (http://www.genome.jp/kegg/) and gene-reaction associations (http://www.enzyme-database.org/)). The model and constraint consistency checker (MC^3) algorithm was used to identify dead-end metabolites, single-connected metabolites, and zero-flux reactions (Yousofshahi et al. 2013). As a result, gaps were identified and as many reactions as possible were added. The biomass reaction was modified to consider 47 molecules of adenosine diphosphate (ADP) and 47 molecules of inorganic phosphate (pi), which are commonly used in genome scale models of *Streptomyces coelicolor* and *Mycobacterium tuberculosis* (Borodina et al. 2005; Jamshidi and Palsson 2007; Alam et al. 2010). The clavam pathway was extended to consider the route of 5s clavams (10 reactions were added in total). Besides, in the transition of clavaminic acid to CA, further reactions of the metabolites N-glycyl-clavaminic acid and N-acetyl-glycyl-clavaminic acid were added (one reaction was removed and three reactions were added in total) (Arulanantham et al. 2006; Ramirez-Malule et al. 2016b). Likewise, a metabolite, named "clavam5s", was added at the end of the 5s clavam route, as this pathway is still under investigation (Zelyas et al. 2008; Ozcengiz and Demain 2013). The exchange and transport reactions for oxaloacetate, clavam-2-carboxylate and alanylclavam were inserted. In summary, a total of 18 reactions were added to the original model of Medema.

The adjusted model consisted of 1510 reactions (1305/205 internal/exchange fluxes) and 1187 metabolites (982/205 internal/external metabolites); it was validated following the standard

protocols reported by Palsson and Lee *et al*. (Palsson 2005; Lee et al. 2009). The SBML version of the full model is available upon request.

Computational tools

The software COBRA Toolbox v2.0 running in a Matlab® environment, using the Gurobi optimization software, was used to solve all optimization problems (Schellenberger et al. 2011).

Results

Continuous cultivation of *S. clavuligerus*

Pre-experimental work was performed at different deceleration rates and dilution rates to guarantee that the system remains at a pseudo-steady state (data not shown). In the final set-up, the dilution rate was varied from 0.050 h^{-1} to 0.025 h^{-1} with a deceleration rate constant of 0.00039 h^{-2}. After the first 36 h of cultivation (batch mode), the culture was kept at a dilution rate of 0.050 h^{-1} for over 4 residence times (τ); a change in cell morphology was observed at the beginning of the continuous feeding mode (pellet formation). After 4τ, the dilution rate was gradually decreased within the next 50 hours to 0.025 h^{-1}.

During the batch phase, a maximum cell dry weight of 10. 45 g/L was obtained at 36 h. Biomass concentration remained rather constant in the subsequent continuous phase at constant dilution rates (see Fig. 2). The availability of glycerol gradually decreased within the following continuous phase with decreasing feed rate (0.092 - 0.020 g/L of glycerol during the dilution rate interval of 0.050 to 0.025 h^{-1}). As a result, the carbon flux through the entire metabolic network might have gradually diminished, leading to a reduction of intermediate metabolite pools, e.g., TCA cycle intermediates along with biomass precursors.

The pellet formation started after the end of the batch phase (continuous mode at 0.05 h^{-1}). Cell stress like nutrient depletion, but also aging effects might cause such a change in morphological behavior, although only a rare number of reports of filamentous organisms describe such relations. Nevertheless, it is clear that the shear rates present in the stirred tank reactor at this study are low enough to support pellet formation. It was shown that the pellet formation is strongly reduced at shear rates above a certain threshold (Kumar and Dubey 2017). It is assumed that the average shear rates, which appear in this small scale cultivation are an order of magnitude lower than what was observed in pilot scale of 500 L (Pinto et al. 2004). If shear rates

of that scale were compared to a tenfold scale of 5 m³, the hyphal area would be doubled. It is unlikely that the low shear forces in this study, compared to shear forces that prevent pellet formation as described in literature, had an impact on the morphologic development. Thus, the deceleration phase is characterized by a pellet morphology with low portion of hyphae on the total biomass.

CA accumulation started after the end of the batch phase. Semi quantitative analysis of phosphate and ammonia proved that the continuous cultivation was phosphate, but not nitrogen limited. Consequently, CA accumulation was mainly caused by phosphate limitation (see supplementary material 1). The highest CA titer was reached at 36 h (Fig. 2). After that, a clear decrease of CA concentration was observed from 36 to 156 h of cultivation time ($D = 0.05$ h^{-1}) (see Fig. 2). At first sight, a decrease of CA concentration was caused by a lower rate of synthesis (of CA) in the continuous mode and/or, by the dilution effect of continuous feeding after the batch phase. However, CA has been reported to be unstable in synthetic buffer solutions (Ramirez-Malule et al. 2016a) and fed-batch cultivations (Roubos et al. 2002). Moreover, CA synthesis stopped when glycerol became the limiting substrate (see Figs. 2 and 3a).

Acetate and TCA cycle intermediate accumulation in continuous cultivation of *S. clavuligerus*

Acetate and succinate were simultaneously accumulated from 36 to 132 h of cultivation (see Fig. 3a). Figure 3b shows the accumulation of oxaloacetate and malate from 36 h of cultivation onwards, and from 132 to 195 h of cultivation, respectively. The highest accumulation of oxaloacetate and malate was acquired in the stage of variation of the dilution rate, with glycerol depletion; this accumulation progressively decreased when the dilution rate was varied from 0.050 h^{-1} to 0.025 h^{-1} (see Fig. 3c).

Acetate and succinate had a constant level of over 1 mM as long as glycerol was available; nonetheless both intermediates were not detectable after glycerol limitation occurred. In contrast, oxaloacetate increased to 4 mM after glycerol became limiting, and stayed high afterwards. Malate was slightly accumulated only during glycerol depletion (Figs. 3a and 3b). This metabolic behavior might be explained by the likely activation of the glyoxylate pathway under glycerol limitation (Chan and Sim 1998; Soh et al. 2001).

Lactate, α-ketoglutarate, pyruvate and formate were not accumulated during the entire cultivations; their concentrations stayed below detection limits.

Extracellular concentrations of aspartate, isoleucine, asparagine and threonine remained at very low concentrations (Figs. 4a and b). Their concentrations remained constant throughout the phase of declining dilution rates, except for aspartate whose concentration increased, possibly due to activation of the glyoxylate shunt under glycerol limitation. In contrast, glutamate concentrations decreased drastically after limitation of glycerol occurred. Interestingly, it accumulated again in the decellerostat phase (Figs. 3a and 4c). Glutamate may serve as a storage component for nitrogen, as the nitrogen to carbon ratio might increase during a reduced dilution rate. Glycine was observed mainly within the same time frame where CA was synthesized (Figs. 2 and 4d); this was expected, as glycine is a co-substrate in at least two reactions of the later steps in the clavam pathway (N-glycyl-clavaminic acid and 8-hydroxyalanylclavam formation) (Arulanantham et al. 2006; Zelyas et al. 2008; Ramirez-Malule et al. 2016b).

Flux Balance Analysis in *S. clavuligerus* at batch stage and at three different dilution rates

FBA was used as a tool to evaluate and explain the experimental observations and to draw a potential association between succinate, oxaloacetate, malate and acetate with CA production. The genome scale model was constrained with data from a medium composition that mimics the one used in experiments (Supplementary material 2). As for identifying the set of metabolic pathways that were favored and disfavored under continuous cultivation of *S. clavuligerus*, and their association with TCA cycle intermediate accumulation and CA production, an *in silico* FBA study was conducted. For the purpose of performing comparative analysis among metabolic flux distributions, four points of the cultivation were selected: one at the batch stage and three at various dilution rates, (0.050, 0.045 and 0.035 h^{-1}). The model was constrained with experimentally determined fluxes of succinate, oxaloacetate, malate, acetate, oxygen, glycerol, carbon dioxide and/or CA. Intermediate metabolic fluxes were quantified by means of a two-stage optimization procedure (Schuetz et al. 2007) as follows: firstly, a linear programming (LP) problem was solved using the maximization of a composite objective function (biomass synthesis and CA production). Secondly, a non-linear programming (NLP) problem was solved while using the minimization of the overall intracellular flux as objective function. The NLP problem formulation included two additional constraints obtained from solving the problem at

stage one. The biomass flux and the intracellular flux of the reaction catalyzed by phosphoenolpyruvate (PEP) carboxylase were used for the batch phase, whereas the biomass flux and the intracellular flux of the reaction driven by isocitrate lyase (ICL) were used for the phase where dilution rate was varied. The above-mentioned additional constraints, used at the second stage, were based on experimental evidence, as found in this work. The use of experimental constraints drastically reduced the solution space for the optimization problem, thus leading to more consistent metabolic phenotypes. This computing environment allowed for calculating the metabolic flux vector for each point - four metabolic scenarios - previously selected in the cultivation. Differences among flux vectors were used to explain experimental observations.

Figure 5 shows the metabolic flux distribution. Table 1 shows a comparison between the observed dilution rates D and the simulated specific growth rates μ_{sim}; experimental metabolic fluxes are also presented. A good agreement between D and μ_{sim}, 10% of difference on average, was observed, thus indicating the general validity of the model.

Since the CA production rate is rather low in contrast to the overall fluxes, its estimated synthesis rate were not considered for discussion. However, an analysis of the main differences found in the metabolic carbon flux distribution between batch stage and the selected dilution rates is presented.

Discussion

In continuous phosphate limited culture, with glycerol as the carbon source, significant changes of precursor accumulation and concomitant flux distributions were observed. However, fluxes from argininosuccinate to clavaminic acid and CA remained rather unchanged.

The effect of phosphate concentration on CA production by *S. clavuligerus* has been well studied (Ives and Bushell 1997; Kirk et al. 2000; Bushell et al. 2006). Nevertheless, the role of accumulation of intermediate metabolites in *S. clavuligerus* cultures for CA production under phosphate limitation has not been reported. Coincidentally, when the glycerol concentration decreased below 3.8 g/L and acetate and succinate concentration were progressively decreasing to zero, a slight increment (~1 g/L) on biomass production was observed at $D = 0.050$ h^{-1} (between 108 and 132 h of cultivation. See Figs. 2 and 3a). Under these circumstances, acetate and succinate might have been co-assimilated by the cell, hence leading to a further biomass

precursor production (see supplementary material 3). In this regard, Chan and Sim (1998) and Soh *et al*. (2001) found a metabolic relationship between the carbon source (either glycerol or acetate), cell growth and isocitrate lyase activity, where, for both glycerol and acetate, high levels of ICL activity coincided with a diminution of growth (Chan and Sim 1998; Soh et al. 2001). Additionally, the authors reported that *S. clavuligerus* was able to grow on acetate as the sole carbon source.

Acetate metabolism is also linked with the formation of N-acetylated clavaminic acid compounds in the clavam pathway. Crystallographic studies and mass spectrometry analysis have shown a close similarity between *orf14* (acetyl transferase (CBG)) and the GCN5-related acetyltransferase (GNAT) protein (Iqbal et al. 2010; Paradkar 2013). Besides, a reaction mechanism for the acetate incorporation during N-acetyl-glycyl-clavaminic acid formation was proposed based on a computational-based approach, a postulated new step in the later steps of the clavam pathway (Ramirez-Malule et al. 2016b).

The role of succinate in anabolic processes of *S. clavuligerus* is a matter of several studies (Dekleva and Strohl 1988; Hodgson 2000). In our experiments, succinate accumulated within a time frame during which CA was synthesized, at a constant dilution rate of 0.05 h^{-1} (succinate: from 36 to 121 h of cultivation, Fig. 3a; CA: from 36 h of cultivation onwards, Fig. 2). Succinate is produced in the TCA cycle; it is also a substrate for fumarate biosynthesis. Additionally, succinate is related with the clavam pathway wherein it is released as a byproduct of three intermediate clavam reactions (see Fig. 1) (Townsend 2002; Ozcengiz and Demain 2013). The enzyme involved in these three reactions is clavaminate synthase, an α-ketoglutarate (α-KG) and ferrous iron-dependent oxygenase. This enzyme catalyzes the following reactions: (i) deoxiguanidino-proclavaminic acid is hydroxylated to guanidine-proclavaminic acid, (ii) proclavaminic acid to dihydroclavaminic acid, (iii) biosynthesis of clavaminic acid (Krol et al. 1989; Salowe et al. 1991; Zhou et al. 1998; Solomon et al. 2000; Zhou et al. 2001; Zhang et al. 2002; Townsend 2002). In cephamycin C biosynthesis, succinate is also released as byproduct by the action of α-KG and a ferrous iron-dependent oxygenase (Ozcengiz and Demain 2013; Hamed et al. 2013). Consequently, the cephamycin C pathway, if active, is a potential source for succinate accumulation. It has been found that *S. clavuligerus* produces CA and cephamycin C simultaneously, either in batch or fed-batch mode (Bellão et al. 2013). In cultures fed with

glycerol, CA production was higher than that of cephamycin C. In contrast, the concentration of cephamycin C was higher than CA when starch was used (Bellão et al. 2013).

Figure 3b shows an accumulation of oxaloacetate at 24 h of cultivation. At this time, oxaloacetate may originate not only from the TCA cycle but also from the PEP carboxylase reaction. Accumulation of oxaloacetate, as precursor for aspartate, eventually lead to higher fluxes within the urea cycle, thereby promoting the production of arginine, the second CA precursor (Haines et al. 2011). In fact, an increase on the concentration of aspartate, isoleucine, asparagine and threonine (amino acids of the oxaloacetate-family (specifically) matched with CA accumulation (Figs. 2, 4a and b). High pools of GAP and arginine might boost the first reaction of the clavam pathway to *L*-N^2-(2-carboxy-ethyl) arginine (Khaleeli et al. 1999; Ozcengiz and Demain 2013). Bushell *et al.* (2006) observed that the yield of CA was increased when asparagine, arginine and/or threonine were fed to chemostat cultivations of *S. clavuligerus*.

Following the analysis, our data show a transition stage from primary to secondary metabolism between 24 and 36 h of cultivation, concurring with a larger accumulation of CA. Apparently, during this period, PEP carboxylase was active and contributed to the accumulation of oxaloacetate (see Fig. 3b) and maximum CA production (at end of batch phase, Fig. 2). Afterwards, PEP carboxylase was likely inhibited by the constant production and accumulation of oxaloacetate and succinate (oxaloacetate: from 36 h of cultivation onwards, Fig. 3b; succinate: from 36 to 121 h of cultivation, Fig. 3a), while the CA concentration was approx. constant (from 36 h of cultivation onwards, Fig. 2). The role of anaplerotic reactions in primary metabolism of *Streptomycetes* has been widely studied (Vorisek et al. 1969; Dekleva and Strohl 1988; Hodgson 2000). Many *Streptomyces* species use PEP carboxylase for the anaplerotic biosynthesis of oxaloacetate, e.g., *Streptomyces aureofaciens* (A14), *Streptomyces* C5 and *Streptomyces coelicolor* A3(2) (A21) (Vorisek et al. 1969; Dekleva and Strohl 1988; Hodgson 2000). Dekleva and Strohl (1988) observed a minor stimulation of PEP carboxylase by fructose 1,6-bisphosphate and AMP in *Streptomyces* C5, whereas oxaloacetate, aspartate, malate, succinate, ATP, citrate and CoASH were reported as severe inhibitors of PEP carboxylase (Dekleva and Strohl 1988). Besides, the transition from primary to secondary metabolism led to activation of PEP carboxylase due to the growing demand of TCA intermediates during antibiotic biosynthesis (Dekleva and Strohl 1988; Hodgson 2000).

Metabolite profiles of this work showed that malate concentration was increasing with glycerol limitation, mostly between the 132 and 156 h of cultivation, at $D = 0.05$ h^{-1} (see Figs. 3a and 3b). After that, when D was decreased, also the malate concentration was decreased as dilution rate went down to 0.025 h^{-1} (see Fig. 3c). The glyoxylate shunt, a bypass in the TCA cycle, retains two carbon dioxide molecules, and contributes to maintain cell metabolism, under limited carbon source availability. Soh *et al*. (2001) found that the maximum isocitrate lyase and malate synthase enzymatic activity, under either acetate or glycerol limitation, as the unique carbon source, occurred at the same time and was not associated with biomass accumulation. The authors suggested that the glyoxylate pathway in *S. clavuligerus* was active under limited carbon source conditions due to the demonstrated isocitrate lyase and malate synthase activities (Soh et al. 2001). Hence, considering the malate and acetate accumulation, observed in this work, we argue that the glyoxylate pathway was active under phosphate limitation and glycerol depletion. Interestingly, the likely activation of the glyoxylate pathway matched with the absence of CA at the period when the dilution rate varied from 0.050 h^{-1} to 0.025 h^{-1}.

Accumulation of TCA cycle intermediates has also been observed in genetically modified *Streptomyces* strains (Viollier et al. 2001; Colombié et al. 2005). Interestingly, the accumulation of succinate, oxaloacetate, malate and acetate found in this work - using a wild type strain - were comparable with levels reported in *Streptomyces ambofaciens* and *Streptomyces coelicolor* strains, which had been subject to genetic modification (Viollier et al. 2001; Colombié et al. 2005).

Regarding the change in cell morphology, as observed in this work (see supplementary material 3), pellet formation has been reported to have a negative effect on antibiotic production. Several reports describe an increased release of antibiotics, when the portion of branched hyphae is larger as if pellet formation is dominant (Qi et al. 2014), as it is the case at elevated shear rates. However, an optimum exists, while production declines if shear rates harm the structures of the filamentous organisms further (Olmos et al. 2013). A threefold increase in lavendamycin methyl ester was observed in *S. flocculus* (Xia et al. 2014). The decrease of CA concentration matched pellet formation during *S. clavuligerus* cultivation at 0.050 h^{-1}. Under the presence of pellet formation, oxygen and nutrient transport to the cells is limited, thus leading to lower CA titers in submerged cultures. In this regard, recent works have reported on the kinetics of pellet growth

along with studies on adding cations or components to prevent/enhance pellet formation (Kumar and Dubey 2017; Kurakake et al. 2017; Osadolor et al. 2017). Pellet formation is mainly influence by pH, substrate and product concentration, and agitation. Kumar and Dubey (2017) recently studied the role of different carbon and nitrogen sources, metals, pH, inoculum volume and agitation rate on pellet formation in *Streptomyces toxytricini*. In that work, the results showed that galactose, ammonium sulfate, sodium nitrate, Cu^{2+}, Zn^{2+}, an inoculum volume higher than 5% (v/v) and agitation rate of 300 rpm triggered a decrease not only in pellet size, but also in biomass. Nevertheless, a relation between pellet size and maximum shear rates still has to be investigated. Although many growth factors have been described (Ser et al. 2016), the observation of the morphologic evolution of a culture under controlled, low shear stress conditions as e.g., in a shake flask, remains to be investigated, since in both, the stirred tank reactors and even bubble columns, a certain shear stress cannot be avoided without a loss of power input (Cerri and Badino 2012).

The FBA simulation results show a slight reduction in the pool of GAP and arginine under the four tested environmental conditions (pool levels stayed approximately constant, considering the significant change in the dilution rate), and an adverse effect on CA biosynthesis (see fluxes of arginine, CA and the reactions where GAP is involved in Fig. 5). This instance was consistent with the decline of α-ketoglutarate carbon flux (76.4%) towards glutamate, a reaction mediated by glutamate dehydrogenase (probably caused by activation of the glyoxylate pathway). Both compounds are direct precursors of the urea cycle where arginine is synthesized. Furthermore, the oxidative activity in the TCA cycle was limited leading to a lower level of TCA cycle intermediates (39.4% and 43.8%, less flux, for isocitrate and α-ketoglutarate, respectively) and an active glyoxylate pathway. Moreover, pools of GAP and arginine - as precursors of the clavam pathway – are bottlenecks for CA synthesis as suggested by (Ives and Bushell 1997). GAP, as a glycolytic intermediate, is highly demanded for glycolysis and gluconeogenesis. Accordingly, GAP availability rather than arginine is commonly considered as rate-limiting for CA production (Ives and Bushell 1997).

FBA results showed that the reaction driven by PEP carboxylase, wherein oxaloacetate is produced from PEP, was not active since the carbon flux through this irreversible reaction was zero, under the three dilution rates evaluated. In contrast, PEP carboxylase was highly active -

with a flux value of 1.773 mmol/(g_{CDW}*h) - at the batch stage where CA acquired its highest yield.

Likewise, a substantial increment of the flux from PEP towards pyruvate was observed during the four evaluated environmental conditions (see pyruvate in Fig. 5). Interestingly, while the metabolic flux mediated by pyruvate kinase incremented, PEP carboxylase was turned off at the three dilution rates evaluated, clearly a presumed tradeoff between pyruvate kinase and PEP carboxylase. Indeed, in the batch stage the highest flux value of PEP carboxylase coincided with the lowest flux value of pyruvate i.e., CA biosynthesis is related with a high PEP carboxylase enzymatic activity and a reduced activity of pyruvate kinase. Undoubtedly, oxaloacetate production, via PEP carboxylase, plays an important role in CA biosynthesis. In a coincident manner, in this work, the accumulation of oxaloacetate, succinate and amino acids from oxaloacetate-family agreed with a larger CA production. The positive influence of amino acids, derived from oxaloacetate, on CA production has been already studied by means of feeding experiments, using aspartate, threonine, isoleucine, glutamate and arginine as supplements, in chemostat cultivation (Bushell et al. 2006).

Regarding the reaction mediated by ICL, the model predicted the experimentally proven activation of the glyoxylate pathway at the interval in which dilution rate was varied; the irreversible reaction catalyzed by ICL was active (see glyoxylate flux in Fig. 5). The activation of ICL was ultimately caused by glycerol and phosphate depletion during the variation of the dilution rate from 0.050 h^{-1} to 0.025 h^{-1}.

As previously highlighted, CA concentration was close to zero at the period when the dilution rate was varied from 0.050 h^{-1} to 0.025 h^{-1}. In this regard, we now analyzed the effect of the possible physiological flux ratio that eventually would regulate carbon flux distribution in early steps of the clavam pathway.

The flux-ratio for aspartate/glutamate had a substantial increment (237% on average, from batch to $D = 0.035$ h^{-1}), thus showing a clear decreasing trend of carbon flux in the oxidative direction of the TCA cycle (see Fig. 6). This instance might be caused mainly by glycerol and phosphate depletion, which triggered the activation of the glyoxylate pathway within the period when the dilution rate was varied. The flux-ratio for aspartate/arginine was rather constant since aspartate

is a direct precursor of arginine. In mammals, the reaction mediated by argininosuccinate synthetase - where citrulline and aspartate condense to form argininosuccinate - has been reported to be the rate-limiting step under circumstances where the urea cycle runs maximally (Haines et al., 2011, Morris Jr, 1992). Then, argininosuccinate synthetase might regulate carbon flux towards the synthesis of arginine, hence rendering an invariable flux-ratio profile for the ratio aspartate/arginine. In contrast, the glutamate/arginine flux-ratio decreased by 71%. Here, the intracellular flux toward glutamate (a reaction mediated by glutamate dehydrogenase where α-ketoglutarate, together with urea, were used as co-substrate), experienced a severe diminution (76.9%), while metabolic flux for aspartate ceased around 20.1%. The trend for the flux-ratio of aspartate/α-ketoglutarate increased moderately. The activation of the glyoxylate shunt allows for producing succinate and malate; the latter is used as substrate to generate oxaloacetate, which is a precursor of aspartate. This instance let to obtain more aspartate than α-ketoglutarate. The lack of succinate accumulation and the absence of CA during the variation of the dilution rate was an indicator of a low activity of the clavam pathway. Certainly, the *in silico* results showed an imbalance between aspartate and glutamate fluxes - when the dilution rate was varied from 0.050 h^{-1} to 0.035 h^{-1} - with a strong negative effect on arginine biosynthesis (see arginine in Figs. 5 and 6).

A clear relationship between aspartate and glutamate with CA production was observed; this association affects TCA cycle intermediate flux distribution. Accordingly, the reactions driven by glutamate dehydrogenase and aspartate aminotransferase could eventually be considered as potential metabolic targets for further genetic modification so as to obtain *S. clavuligerus* over-producer strains.

Finally, findings in this study have shown a strong association between the accumulation of succinate, oxaloacetate, malate and acetate with CA production in *S. clavuligerus.* The reaction catalyzed by PEP carboxylase was consistent with oxaloacetate accumulation and the highest CA production. Furthermore, CA biosynthesis coincided with the accumulation of oxaloacetate, succinate and acetate during the initial batch phase, and at a dilution rate of 0.050 h^{-1}. In contrast, when CA was depleted, malate was accumulated just before starting the variation of dilution rate and at the point when D decreased to 0.025 h^{-1}. These results demonstrated the existence of a metabolic relationship between the accumulation of TCA intermediates and CA production,

which gives rise to potential metabolic targets for obtaining a desired CA-overproducing strain; as previously stated, the reactions conducted by glutamate dehydrogenase and aspartate aminotransferase might be potential candidates for this purpose.

Acknowledgments

H.R.M. thanks Prof. Sven-Olof Enfors and Victor Lopez-Agudelo for valuable discussions about *in silico* simulations. The authors thank Prof. Dr. Rainer Breitling (University of Manchester, England) for providing a genome-scale model of *S. clavuligerus,* reported by Medema et al. (2010).

Funding Information: The authors kindly acknowledge the support of the Federal German Ministry of Education and Research and Departamento Administrativo de Ciencias, Tecnología e Innovación - COLCENCIAS, grant no. 01DN16018. The German Academic Exchange Service (DAAD) funded the contribution of H.R.M., grant number A/13/71981.

Compliance with Ethical Standards

Conflict of interest: The authors declare that they have no conflict of interest

Ethical Approval: This article does not contain any studies with human participants or animal performed by any of the authors.

References

Alam MT, Merlo ME, Consortium TS, Hodgson DA, Wellington EMH, Takano E, Breitling R (2010) Metabolic modeling and analysis of the metabolic switch in *Streptomyces coelicolor*. BMC Genomics 11:202.

Antoniewicz MR (2015) Methods and advances in metabolic flux analysis: a mini-review. J Ind Microbiol Biotechnol 42:317–325.

Arulanantham H, Kershaw NJ, Hewitson KS, Hughes CE, Thirkettle JE, Schofield CJ (2006) ORF17 from the clavulanic acid biosynthesis gene cluster catalyzes the ATP-dependent formation of N-glycyl-clavaminic acid. J Biol Chem 281:279–87.

Bachmann B, Li R, Townsend C (1998) beta-Lactam synthetase: a new biosynthetic enzyme. Proc Natl Acad Sci U S A 95:9082–6.

Bellão C, Antonio T, Araujo MLGC, Badino AC (2013) Production of clavulanic acid and cephamycin c by *Streptomyces clavuligerus* under different fed-batch conditions. Brazilian J Chem Eng 30:257–266.

Borodina I, Krabben P, Nielsen J (2005) Genome-scale analysis of *Streptomyces coelicolor* A3(2) metabolism. Genome Res 15:820–9.

Brown A., Butterworth D, Cole M, Hanscomb G, Hood J., Reading C, Rolinson G. (1976) Naturally Occurring β-lactamase Inhibitors with Actibacterial Activity. J Antibiot (Tokyo) 29:668–669.

Bushell ME, Kirk S, Zhao H-J, Avignone-Rossa CA (2006) Manipulation of the physiology of clavulanic acid biosynthesis with the aid of metabolic flux analysis. Enzyme Microb Technol 39:149–157.

Cerri MO, Badino AC (2012) Shear conditions in clavulanic acid production by *Streptomyces clavuligerus* in stirred tank and airlift bioreactors. Bioprocess Biosyst Eng 35:977–984.

Chan M, Sim T (1998) Malate synthase from *Streptomyces clavuligerus* NRRL3585: cloning, molecular characterization and its control by acetate. Microbiology 144:3229–3237.

Colombié V, Bideaux C, Goma G, Uribelarrea JL (2005) Effects of glucose limitation on biomass and spiramycin production by *Streptomyces ambofaciens*. Bioprocess Biosyst Eng 28:55–61.

Dekleva ML, Strohl WR (1988) Activity of phosphoenolpyruvate carboxylase of an anthracycline-producing streptomycete. Can J Microbiol 34:1241–1246.

Foulstone M, Reading C (1982) Assay of amoxicillin and clavulanic acid, the components of Augmentin, in biological fluids with high-performance liquid chromatography. Antimicrob Agents Chemother 22:753–762.

Haines RJ, Pendleton LC, Eichler DC (2011) Argininosuccinate synthase: at the center of arginine metabolism. Int J Biochem Mol Biol 2:8–23.

Hamed RB, Gomez-Castellanos JR, Henry L, Ducho C, McDonough MA, Schofield CJ (2013) The enzymes of β-lactam biosynthesis. Nat Prod Rep 30:21–107.

Hodgson D a (2000) Primary metabolism and its control in streptomycetes: a most unusual group of bacteria. Adv Microb Physiol 42:47–238.

Hwang K-S, Kim HU, Charusanti P, Palsson BØ, Lee SY (2014) Systems biology and biotechnology of *Streptomyces* species for the production of secondary metabolites. Biotechnol Adv 32:255–68.

Iqbal A, Arunlanantham H, Brown T, Chowdhury R, Clifton IJ, Kershaw NJ, Hewitson KS, McDonough MA, Schofield CJ (2010) Crystallographic and mass spectrometric analyses of a tandem GNAT protein from the clavulanic acid biosynthesis pathway. Proteins 78:1398–407.

Ives PR, Bushell ME (1997) Manipulation of the physiology of clavulanic acid production in *Streptomyces clavuligerus*. Microbiology 143:3573–9.

Jamshidi N, Palsson BØ (2007) Investigating the metabolic capabilities of *Mycobacterium tuberculosis* H37Rv using the in silico strain iNJ661 and proposing alternative drug targets. BMC Syst Biol 1:26.

Junne S, Klingner A, Kabisch J, Schweder T, Neubauer P (2011) A two-compartment bioreactor system made of commercial parts for bioprocess scale-down studies: impact of oscillations on *Bacillus subtilis* fed-batch cultivations. Biotechnol J 6:1009–17.

Khaleeli N, Li R, Townsend C a. (1999) Origin of the β-lactam carbons in clavulanic acid from an unusual thiamine pyrophosphate-mediated reaction. J Am Chem Soc 121:9223–9224.

Kirk S, Avignone-rossa CA, Bushell ME (2000) Growth limiting substrate affects antibiotic production and associated metabolic fluxes in *Streptomyces clavuligerus*. Biotechnol Lett 22:1803–1809.

Krol WJ, Basak A, Salowe SP, Townsend C a. (1989) Oxidative cyclization chemistry catalyzed by clavaminate synthase. J Am Chem Soc 111:7625–7627.

Kumar P, Dubey KK (2017) Mycelium transformation of *Streptomyces toxytricini* into pellet: Role of culture conditions and kinetics. Bioresour Technol 228:339–347.

Kurakake M, Hirotsu S, Shibata M, Takenaka Y, Kamioka T, Sakamoto T (2017) Effects of nonionic surfactants on pellet formation and the production of β-fructofuranosidases from *Aspergillus oryzae* KB. Food Chem 224:139–143.

Lee S, Song H, Kim T, Sohn S (2009) Validation of metabolic models. In: Smolke C (ed) The Metabolic Pathway Engineering Handbook: Fundamentals, First edit. CRC Press, Taylor & Francis Group, p 20.1-20.12

Lemoine A, Limberg MH, Kästner S, Oldiges M, Neubauer P, Junne S (2016) Performance loss of *Corynebacterium glutamicum* cultivations under scale-down conditions using complex media. Eng Life Sci 16:620–632.

Lemoine A, Maya Martnez-Iturralde N, Spann R, Neubauer P, Junne S (2015) Response of *Corynebacterium glutamicum* exposed to oscillating cultivation conditions in a two- and a novel three-compartment scale-down bioreactor. Biotechnol Bioeng 112:1220–1231.

Llarrull LI, Testero S a, Fisher JF, Mobashery S (2010) The future of the β-lactams. Curr Opin Microbiol 13:551–557.

Medema MH, Trefzer A, Kovalchuk A, van den Berg M, Müller U, Heijne W, Wu L, Alam MT, Ronning CM, Nierman WC, Bovenberg R a L, Breitling R, Takano E (2010) The sequence of a 1.8-mb bacterial linear plasmid reveals a rich evolutionary reservoir of secondary metabolic pathways. Genome Biol Evol 2:212–24.

Neto AB, Hirata DB, Filho LCMC, Bellão C, Júnior ACB, Hokka CO (2005) A study on clavulanic acid production by *Streptomyces clavuligerus* in batch , fed-batch and continuous processes. Brazilian J Chem Eng 22:557–563.

Olmos E, Mehmood N, Haj Husein L, Goergen JL, Fick M, Delaunay S (2013) Effects of bioreactor hydrodynamics on the physiology of *Streptomyces*. Bioprocess Biosyst Eng 36:259–272.

Osadolor OA, Nair RB, Lennartsson PR, Taherzadeh MJ (2017) Empirical and experimental determination of the kinetics of pellet growth in filamentous fungi: A case study using Neurospora intermedia. Biochem Eng J 124:115–121.

Ozcengiz G, Demain AL (2013) Recent advances in the biosynthesis of penicillins,

cephalosporins and clavams and its regulation. Biotechnol Adv 31:287–311.

Paalme T, Kahru Anne, Elken R, Vanatalu K, Tiisma K, Vilu R (1995) The computer-controlled continuous culture of *Escherichia coli* with smooth change of dilution rate (A-stat). J Microbiol Methods 24:145–153.

Palsson B (2005) Systems Biology: Properties of Reconstructed Networks. Cambridge University Press

Paradkar A (2013) Clavulanic acid production by *Streptomyces clavuligerus*: biogenesis, regulation and strain improvement. J Antibiot (Tokyo) 66:411–20.

Pinto LS, Vieira LM, Pons MN, Fonseca MMR, Menezes JC (2004) Morphology and viability analysis of *Streptomyces clavuligerus* in industrial cultivation systems. Bioprocess Biosyst Eng 26:177–184.

Qi H, Zhao S, Fu H, Wen J, Jia X (2014) Coupled cell morphology investigation and metabolomics analysis improves rapamycin production in *Streptomyces hygroscopicus*. Biochem Eng J 91:186–195.

Ramirez-Malule H, Junne S, López C, Zapata J, Sáez A, Neubauer P, Rios-Estepa R (2016a) An improved HPLC-DAD method for clavulanic acid quantification in fermentation broths of *Streptomyces clavuligerus*. J Pharm Biomed Anal 120:241–247.

Ramirez-Malule H, Restrepo A, Cardona W, Junne S, Neubauer P, Rios-Estepa R (2016b) Inversion of the stereochemical configuration (3S,5S)-clavaminic acid into (3R,5R)-clavulanic acid: A computationally-assisted approach based on experimental evidence. J Theor Biol 395:40–50.

Roubos JA (2002) Bioprocesses modeling and optimization fed-batch clavulanic acid production by *Streptomyces clavuligerus*. Dissertation, Technische Universiteit Delft

Roubos JA, Krabben P, De Laat W, Heijnen JJ (2002) Clavulanic acid degradation in *Streptomyces clavuligerus* fed-batch cultivations. Biotechnol Prog 18:451–457.

Salowe SP, Krol WJ, Iwata-Reuyl D, Townsend C a. (1991) Elucidation of the order of oxidations and identification of an intermediate in the multistep clavaminate synthase reaction. Biochemistry 30:2281–2292.

Schellenberger J, Que R, Fleming RMT, Thiele I, Orth JD, Feist AM, Zielinski DC, Bordbar A, Lewis NE, Rahmanian S, Kang J, Hyduke DR, Palsson BØ (2011) Quantitative prediction of cellular metabolism with constraint-based models: the COBRA Toolbox v2.0. Nat Protoc 6:1290–307.

Schuetz R, Kuepfer L, Sauer U (2007) Systematic evaluation of objective functions for predicting intracellular fluxes in *Escherichia coli*. Mol Syst Biol 3:119.

Ser H, Law JW, Chaiyakunapruk N, Jacop SA, Palanisamy UD, Chan K-G, Goh B-H, Lee L (2016) Fermentation conditions that affect clavulanic acid production in *Streptomyces clavuligerus*: a systematic review. Front Microbiol.

Soh BS, Loke P, Sim T (2001) Cloning, heterologous expression and purification of an isocitrate lyase from *Streptomyces clavuligerus* NRRL 3585. Biochim Biophys Acta 1522:112–117.

Solomon EI, Brunold TC, Davis MI, Kemsley JN, Lee S-K, Lehnert N, Neese F, Skulan AJ, Yang Y-S, Zhou J (2000) Geometric and electronic structure/function correlations in non-heme iron enzymes. Chem Rev 100:235–350.

Stephanopoulos G, Aristidou A, Nielsen J (1998) Metabolic Engineering. Principles and Methodologies. Academic press, USA

Townsend C a (2002) New reactions in clavulanic acid biosynthesis. Curr Opin Chem Biol 6:583–9.

Villadsen J, Nielsen J, Lidén G (2011) Bioreaction Engineering Principles, Third. Springer

Viollier PH, Minas W, Dale GE, Folcher M, Thompson CJ (2001) Role of acid metabolism in *Streptomyces coelicolor* morphological differentiation and antibiotic biosynthesis. J Bacteriol 183:3184–3192.

Vorisek J, Powell A, Vanek Z (1969) Regulation of biosynthesis of secondary metabolites iv. purification and properties of phosphoenolpyruvate carboxylase in *Streptomyces aureofaciens*. Folia Microbiol (Praha) 14:398–405.

Wu TK, Busby RW, Houston TA, Mcilwaine DB, Egan LA, Townsend CA, Wu T, Busby RW, Houston TA, Ilwaine DBMC, Egan LA, Townsend CA (1995) Identification, Cloning, Sequencing, and overexpression of the gene encoding proclavaminate amidino hydrolase

and characterization of protein function in clavulanic acid biosynthesis. J Bacteriol 177:3714–3720.

Xia X, Lin S, Xia XX, Cong FS, Zhong JJ (2014) Significance of agitation-induced shear stress on mycelium morphology and lavendamycin production by engineered *Streptomyces flocculus*. Appl Microbiol Biotechnol 98:4399–4407.

Yousofshahi M, Ullah E, Stern R, Hassoun S (2013) MC3: a steady-state model and constraint consistency checker for biochemical networks. BMC Syst Biol 7:129.

Zelyas NJ, Cai H, Kwong T, Jensen SE (2008) Alanylclavam biosynthetic genes are clustered together with one group of clavulanic acid biosynthetic genes in *Streptomyces clavuligerus*. J Bacteriol 190:7957–65.

Zhang Z, Ren JS, Harlos K, McKinnon CH, Clifton IJ, Schofield CJ (2002) Crystal structure of a clavaminate synthase-Fe(II)-2-oxoglutarate-substrate-NO complex: evidence for metal centered rearrangements. FEBS Lett 517:7–12.

Zhou J, Gunsior M, Bachmann BO, Townsend CA, Solomon EI (1998) Substrate binding to the α-ketoglutarate-dependent non-heme iron enzyme clavaminate synthase 2: coupling mechanism of oxidative decarboxylation and hydroxylation. J Am Chem Soc 120:13539–13540.

Zhou J, Kelly WL, Bachmann BO, Gunsior M, Townsend CA, Solomon EI (2001) Spectroscopic studies of substrate interactions with clavaminate synthase 2 , a multifunctional α-kg-dependent non-heme iron enzyme : correlation with mechanisms and reactivities spectroscopic studies of substrate interactions with clavaminate synthase 2. J Am Chem Soc 123:7388–7398.

Table Legends

Table 1 Observed dilution rates from continuous cultivation and experimental and simulated specific growth rates of *S. clavuligerus*.

Figures Legends

Fig. 1 A condensed scheme of the clavam pathway in *S. clavuligerus*. Succinate is a byproduct in three reactions catalyzed by clavaminic acid synthase in the presence of α-ketoglutarate (a-KG) and an iron-dependent oxygenase

Fig. 2 Continuous cultivation of *S. clavuligerus*: Cell dry weight (-▲-) and (-●-) clavulanic acid concentration as a function of cultivation time. Numbers above pictures describe the portion of pixels, which depict biomass

Fig. 3 Accumulation of tricarboxylic acid cycle intermediates during continuous cultivation of *S. clavuligerus*. **a)** Time course of glycerol consumption (-▲-), and accumulation of succinate (-●-) and acetate (-■-) in continuous cultivation of *S. clavuligerus.* **b)** Concentration of oxaloacetate (-▲-) and malate (-●-) during continuous cultivation of *S. clavuligerus*. **c)** Accumulation of oxaloacetate (-▲-) and malate (-●-) from 0.050 h^{-1} to 0.025 h^{-1} of dilution rate in continuous cultivation of *S. clavuligerus*

Fig. 4 Course of extracellular concentration of amino acids in continuous cultivation of *S. clavuligerus*: **a)** Aspartate (-▲-) and isoleucine (-●-). **b)** Asparagine (-▲-) and threonine (-●-). **c)** Glutamate (-▲-) and glutamine (-●-). **d)** Glycine (-▲-) and arginine (-●-)

Fig. 5 Carbon flux distribution in CA production by *S. clavuligerus*, at batch stage and at three different dilution rates. Units for fluxes are mmol/(g_{CDW}*h). Notation: from top to down, flux values correspond to a metabolic flux distribution of *S. clavuligerus* growing in batch culture (36 h of cultivation), and three selected dilution rates 0.050, 0.045 and 0.035 h^{-1}, within the continuous mode, at 155, 180 and 195 h of cultivation, respectively

Fig. 6 Flux ratio profiles for the intracellular fluxes of aspartate (ASP), glutamate (GLU), α-ketoglutarate (a-KG) and arginine (ARG). Notation: The flux ratio values correspond to data from a metabolic flux distribution of a continuous cultivation at 36 h of cultivation (end of batch stage) and three selected dilution rates (0.050, 0.045 and 0.035 h^{-1})

Table 1

Table 1 Observed dilution rates from continuous cultivation and experimental and simulated specific growth rates of *S. clavuligerus*.

Compounds used as constraints	**Observed dilution rate *D* (h^{-1}), experimental, μ (h^{-1}), and simulated specific growth rate, μ_{sim} (h^{-1})**							
	Batch stage		**Continuous mode**					
	μ	**μ_{sim}**	**D**	**μ_{sim}**	**D**	**μ_{sim}**	**D**	**μ_{sim}**
	0.063	0.054	0.050	0.050	0.045	0.045	0.035	0.044
	Metabolic fluxes*							
Glycerol	-		0.7280		1.1098		0.9679	
O_2	-		1.8481		1.6648		1.6205	
CO_2	-		0.2529		0.0672		0.0228	
Malate	0.0016		0.0016		0.0057		0	
Succinate	0.0140		0		0		0	
Acetate	0.0150		0		0		0	
Oxaloacetate	0.0007		0.0440		0.0291		0	

*Flux units [mmol/(g_{CDW}*h)]. All fluxes were experimentally quantified and used as constraints for simulation purposes. *D* or μ were compared with μ_{sim}. The specific growth rate μ was determined according to eq. 5 (for the batch stage). The observed dilution rate was quantified by the quotient of real medium flow rate (F) and real reactor volume (V), $\left(D = \frac{F}{V}\right)$.

Figure 1

Click here to download Figure Fig 1.tif

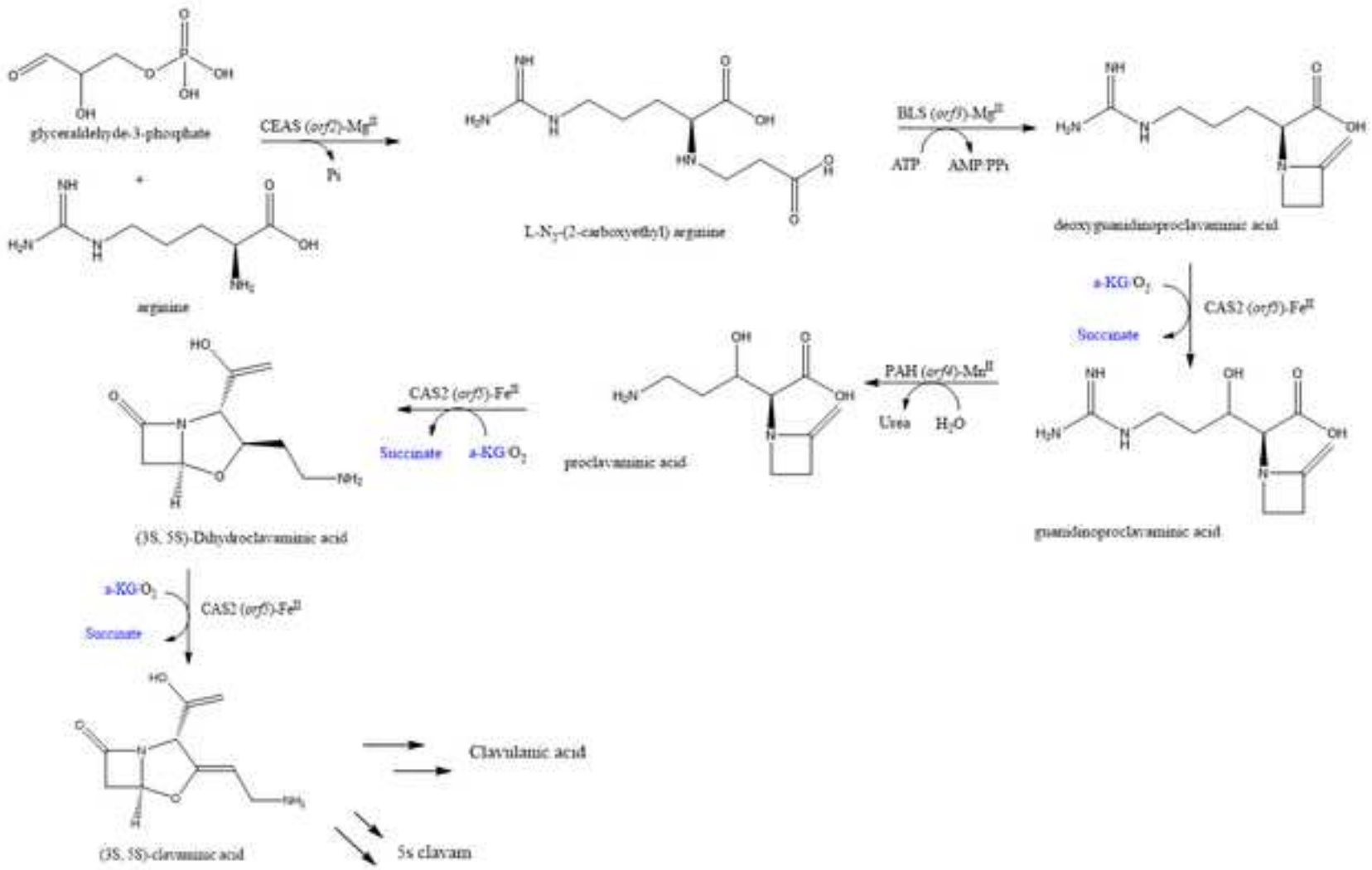

Figure 2

Click here to download Figure Fig 2.tif

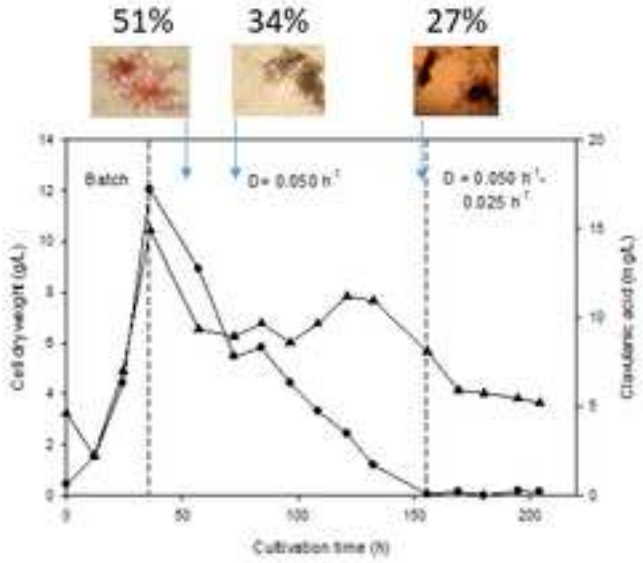

Figure 3

Click here to download Figure Fig 3.tif

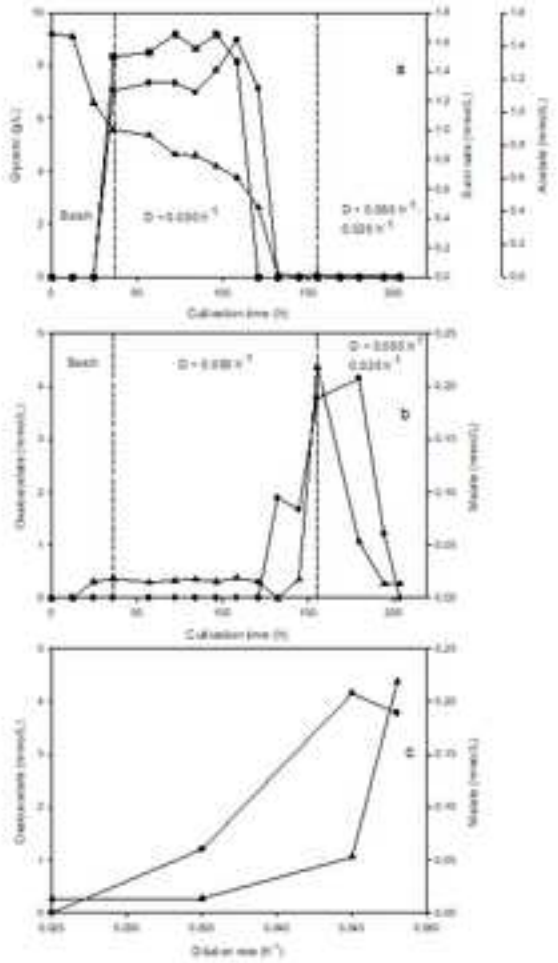

Figure 4

Click here to download Figure Fig 4.tif

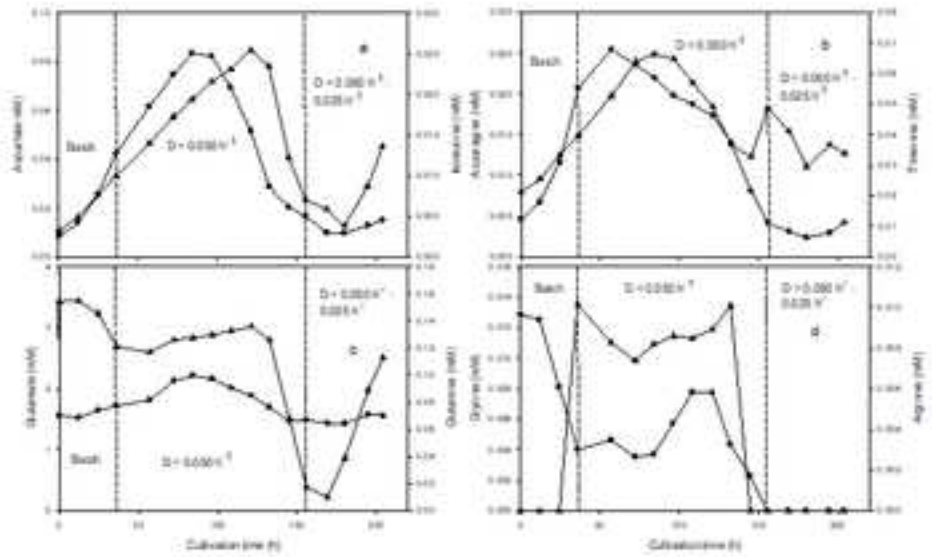

Figure 5

Click here to download Figure Fig 5.tif

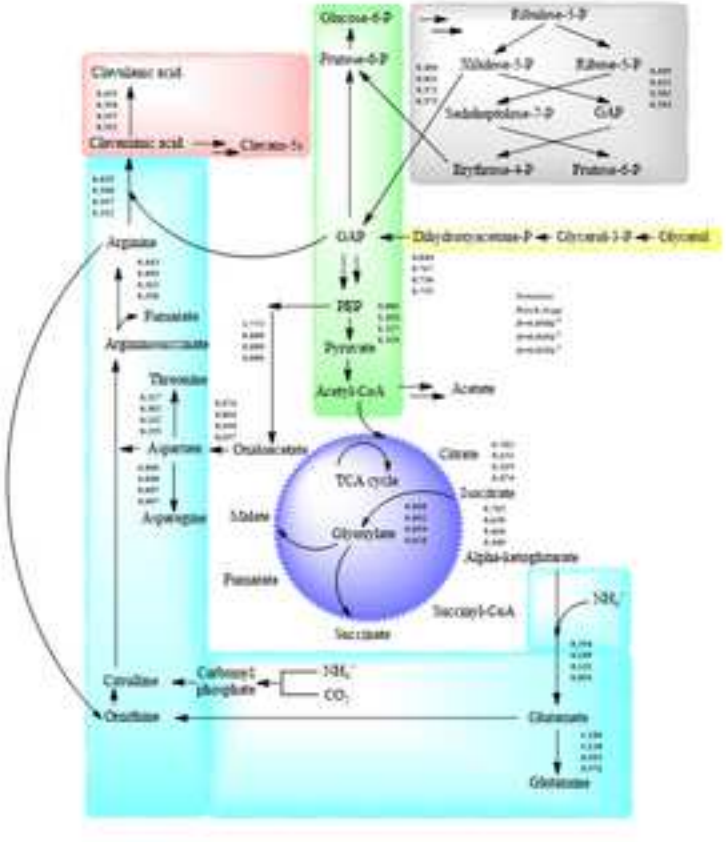

Figure 6

Click here to download Figure Fig 6.tif